INTERNATIONAL JOURNAL FOR NUMERICAL METHODS IN FLUIDS, VOL. 10, 13–34 (1990)

A FINITE ELEMENT SOLUTION OF UNSTEADY TWO-DIMENSIONAL FLOW IN CASCADES

D. S. WHITEHEAD*

Whittle Laboratory, Cambridge University Engineering Department, Madingley Road, Cambridge, U.K.

SUMMARY

A theory is presented for unsteady two-dimensional potential transonic flow in cascades of compressor and turbine blades using a mesh of triangular finite elements. The theory leads to a computer program, FINSUP, which is fast and has moderate storage requirements, so that it can be run on a personal computer. Comparisons with other theories in special cases show that the program is accurate in subsonic flow, and that in supersonic flow, although the wave effects are smeared by the numerical process, the results for overall blade force and moment have acceptable accuracy. The program is useful for engineering assessment of unstalled flutter of actual compressor and turbine blades.

KEY WORDS Blade-vibration Aero-elasticity Flutter

INTRODUCTION

The overall aim of the present paper is to predict flutter in the blades of axial flow compressors and turbines. For this purpose it is required to calculate the unsteady aerodynamic forces and moments on the blades due to their vibration. The method to be used is essentially two-dimensional, but a gradual variation of the thickness (h) of the stream surface will be allowed. The flow will be assumed to be reversible adiabatic flow of a perfect gas. Therefore only weak shock waves can be simulated, and there are no boundary layers or effects due to stalling of the blades. The flow will be assumed to be irrotational, so that a velocity potential (ϕ) exists. This means that the effect of moving wakes coming into the cascade cannot be treated. The flow may be subsonic in some parts of the field and supersonic in other parts. The blade sections are assumed to vibrate with small amplitude as rigid bodies, and with all blades moving identically except for a constant phase shift (β) between each blade and the one above.

Computational methods for the solution of this problem have been reviewed by Whitehead[1] and by Acton and Newton.[2] The governing differential equation is linear, but with variable coefficients. Linearized methods can only be used for small perturbations of a uniform flow, and singularity methods can only be used for incompressible flow. It is therefore necessary to go to a field method. Time-marching methods have been much used but are expensive on computer time. The method described here uses direct matrix division: this leads to a program which is expensive on storage, so that only rather coarse grids can be used, but is fast.

The complete set of programs is called FINSUP. The mesh generation and steady flow calculation have been described by Whitehead and Newton.[3] This report describes the unsteady

* Present address: Inwoods, Farleigh Wick, Bradford-on-Avon, Wiltshire, U.K.

0271–2091/90/010013–22$11.00
© 1990 by John Wiley & Sons, Ltd.
Received 4 October 1988
Revised 9 March 1989

calculation. Several somewhat different versions of this program now exist. An earlier version has been described by Whitehead.[4] The version particularly described here runs on a personal computer. FINSUP has been extended to quasi-three-dimensional flow effects by Cedar and Stow,[5] to blade design by Cedar and Stow[6] and by Hart and Whitehead,[7] and has been coupled into a boundary layer calculation by Stow and Newman.[8]

MESH GENERATION

A typical mesh is shown in Figure 1. It consists of triangular elements covering an area one blade spacing (s) in height, with a blade profile of chord c in the middle, and extending some distance upstream of the leading edge and downstream of the trailing edge. Axes x and y are taken in the axial and tangential directions. Corresponding nodes on the top and bottom of the domain have the same x-co-ordinate. A cusp is added to the profile at the trailing edge to simulate the wake flow here. The ray from the trailing edge is aligned with the expected mean outlet flow direction, and there is a discontinuity of potential across this wake line. The mesh-generating program is arranged to pack elements more thickly in regions of most interest, such as round the leading edge. More details of the mesh generation have been given by Whitehead and Newton.[3]

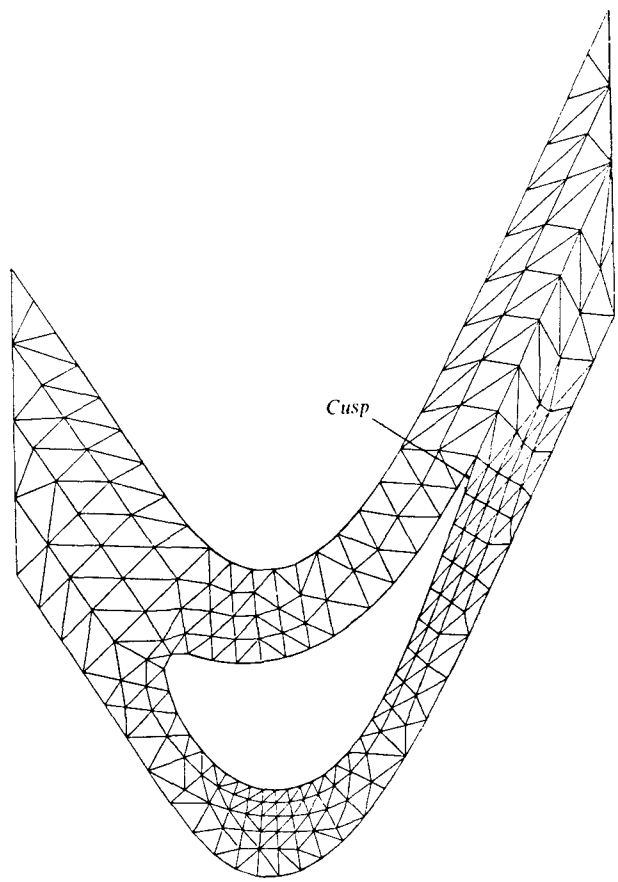

Figure 1. Example of mesh

Within each triangular element a shape function Z_l is defined, which is unity at node l, zero at the other two nodes, and is a linear function of position within the element. Its derivative is given by

$$\frac{\partial Z_l}{\partial x_i}=\frac{1}{2A}\begin{bmatrix}(y_2-y_3) & (y_3-y_1) & (y_1-y_2)\\ (x_3-x_2) & (x_1-x_3) & (x_2-x_1)\end{bmatrix}, \tag{1}$$

where A is the area of the element.

STEADY FLOW CALCULATION

Only the basic equations needed for reference will be given here. Details of the steady flow calculation are given by Whitehead and Newton.[3]

The notation is that p is pressure, ρ is density, u is velocity and q is specific mass flow within a stream tube of height h. An overbar refers to the steady component of any quantity and a prime refers to the unsteady perturbation. Contracted notation is employed, so that summation over all values of a repeated suffix is implied.

The momentum equation is

$$\frac{1}{\bar{\rho}}\frac{\partial \bar{p}}{\partial x_i}+\bar{u}_j\frac{\partial \bar{u}_i}{\partial x_j}=0. \tag{2}$$

For zero vorticity

$$\frac{\partial \bar{u}_i}{\partial x_j}-\frac{\partial \bar{u}_j}{\partial x_i}=0. \tag{3}$$

The flow is given by

$$\bar{q}_i=\bar{\rho}h\bar{u}_i. \tag{4}$$

The continuity equation is

$$\frac{\partial \bar{q}_i}{\partial x_i}=0. \tag{5}$$

UNSTEADY FLOW THEORY

Small unsteady perturbations are now superimposed on the known steady flow. The perturbations are sinusoidal in time (t) with angular frequency (ω), so that all unsteady terms are complex numbers proportional to $\exp(i\omega t)$.

The unsteady velocity is given by

$$u_i'=\frac{\partial \phi'}{\partial x_i}. \tag{6}$$

The deflection of the reference blade due to its vibration is, at a point x_k, given by

$$\zeta_i=\xi_i+\varepsilon_{ijk}\alpha_j x_k, \tag{7}$$

where ξ is the translational deflection of the blade at the origin, ε_{ijk} is the alternating tensor and α_j is the torsional deflection (positive anticlockwise) about this point. ζ_i has components $(\xi_x-\alpha y, \xi_y+\alpha x)$. Its derivative is given by

$$\frac{\partial \zeta_i}{\partial x_k}=\varepsilon_{ijk}\alpha_j, \tag{8}$$

and in particular

$$\frac{\partial \zeta_i}{\partial x_i}=0. \tag{9}$$

The boundary condition at the blade surface is that there is no flow through the displaced and moving surface. The boundary condition to be applied at the mean position of the surface is then

$$n_i q_i' = n_i\left(\bar{\rho}h\frac{\partial \zeta_i}{\partial t}-\varepsilon_{ijk}\alpha_j\bar{q}_k-\zeta_k\frac{\partial \bar{q}_i}{\partial x_k}\right), \tag{10}$$

where n_i is the outward normal to the surface. The first term on the right-hand side is the flow due to the surface velocity, the second term is due to the relative rotation of the blade and the mean flow, and the third term is due to the translation of the matching point through the mean flow field.

A similar consideration applies to the calculation of the unsteady pressure on the surface of the blade, which is given by

$$p_s' = p' + \zeta_k\frac{\partial \bar{p}}{\partial x_k}, \tag{11}$$

where p' is the pressure at the mean position and the last term is due to translation through the mean pressure field. The last terms in equations (10) and (11) have caused numerical difficulty, because round the leading edge the mean flow and mean pressure vary rapidly with position. To overcome this, a modified potential ϕ'' is used. To define this it is noted that the vector ζ_i may be specified by equation (7) over the whole domain of calculation and not just at the blade surface. Then

$$\phi'' = \phi' + \zeta_i\bar{u}_i. \tag{12}$$

The second term in this equation is just the effect of displacing and turning the mean flow to follow the motion of the blade.

The pressure perturbation is then given by

$$p' = -\bar{\rho}\left(\frac{\partial}{\partial t}+\bar{u}_i\frac{\partial}{\partial x_i}\right)\phi' = -\bar{\rho}\left(\frac{\partial}{\partial t}+\bar{u}_i\frac{\partial}{\partial x_i}\right)\left(\phi''-\zeta_k\bar{u}_k\right). \tag{13}$$

The density perturbation is given by

$$\rho' = \frac{p'}{\bar{a}^2} = -\frac{\bar{\rho}}{\bar{a}^2}\left(\frac{\partial}{\partial t}+\bar{u}_i\frac{\partial}{\partial x_i}\right)(\phi''-\zeta_k\bar{u}_k), \tag{14}$$

where a is the speed of sound.

The pressure perturbation at the blade surface is, from equations (11) and (13), and using (2) and (3),

$$p_s' = -\bar{\rho}\left(\frac{\partial \phi''}{\partial t}+\bar{u}_i\frac{\partial \phi''}{\partial x_i}-\bar{u}_i\frac{\partial \zeta_i}{\partial t}\right). \tag{15}$$

This does not contain the awkward derivative of the mean pressure field.

It is also convenient to write

$$q_i'' = q_i' + \zeta_k\frac{\partial \bar{q}_i}{\partial x_k}+\bar{q}_k\frac{\partial \zeta_k}{\partial x_i}-\bar{\rho}h\frac{\partial \zeta_i}{\partial t}, \tag{16}$$

which is the flow vector referred to axes which move with the blade. So the boundary condition at the blade surface becomes simply

$$n_i q_i'' = 0, \tag{17}$$

which does not contain the awkward derivative of the mean flow field.

The expression for q_i'' in terms of ϕ'' and ζ is

$$q_i'' = h\bar{\rho}\left(\delta_{ij} - \frac{\bar{u}_i\bar{u}_j}{\bar{a}^2}\right)\frac{\partial \phi''}{\partial x_j} - \frac{\mathrm{i}\omega h\bar{\rho}}{a^2}\bar{u}_i\phi'' - \mathrm{i}\omega h\bar{\rho}\left(\delta_{ij} - \frac{\bar{u}_i\bar{u}_j}{\bar{a}^2}\right)\zeta_j + \bar{\rho}\bar{u}_i\zeta_j\frac{\partial h}{\partial x_j}, \tag{18}$$

where δ is the substitution tensor.

The unsteady flow perturbation is given by

$$q_i' = (\bar{\rho}u_i' + \bar{u}_i\rho')h. \tag{19}$$

The continuity equation is

$$\frac{\partial q_i'}{\partial x_i} + h\frac{\partial \rho'}{\partial t} = 0. \tag{20}$$

This may be written in terms of q_i'' and ϕ'' as follows:

$$\frac{\partial q_i''}{\partial x_i} - \frac{\mathrm{i}\omega h\bar{\rho}}{\bar{a}^2}\left(\mathrm{i}\omega + \bar{u}_i\frac{\partial}{\partial x_i}\right)\phi'' - \frac{\omega^2 h\bar{\rho}}{\bar{a}^2}\zeta_k\bar{u}_k + \mathrm{i}\omega\bar{\rho}\zeta_i\frac{\partial h}{\partial x_i} = 0. \tag{21}$$

FINITE ELEMENT ANALYSIS

It is assumed that ϕ'' varies linearly within each triangular element. Hence

$$\phi'' = \phi_m'' Z_m, \tag{22}$$

where ϕ_m'' is the value of ϕ'' at node m. This implies that velocities, pressure and density are constant within each element.

To obtain the numerical solution, a Galerkin procedure is used. The continuity equation (21) for each element is multiplied by the shape function Z_l and integrated over the element to give

$$\int\left\{\frac{\partial q_i''}{\partial x_i} - \frac{\mathrm{i}\omega h\bar{\rho}}{\bar{a}^2}\left(\mathrm{i}\omega + \bar{u}_i\frac{\partial}{\partial x_i}\right)\phi'' - \frac{\omega^2 h\bar{\rho}}{\bar{a}^2}\xi_k\bar{u}_k + \mathrm{i}\omega\bar{\rho}\zeta_i\frac{\partial h}{\partial x_i}\right\}Z_l\,\mathrm{d}A = 0. \tag{23}$$

In order to shift the differentiation from the q_i'' term to the 'well behaved' shape function, the first term may be written

$$\int\left\{\frac{\partial}{\partial x_i}(q_i'' Z_l) - q_i''\frac{\partial Z_l}{\partial x_i}\right\}\mathrm{d}A = \int q_i'' n_i Z_l\,\mathrm{d}s - \int q_i''\frac{\partial Z_l}{\partial x_i}\mathrm{d}A, \tag{24}$$

by Gauss' theorem, where n_i is the unit normal drawn out from the surface, and the first integral is taken clockwise round the boundary of the element. Putting this into equation (23) and using (18) gives

$$\begin{aligned}
&\int\left\{\left(\delta_{ij} - \frac{\bar{u}_i\bar{u}_j}{\bar{a}^2}\right)\frac{\partial Z_l}{\partial x_i}\frac{\partial Z_m}{\partial x_j} - \frac{\mathrm{i}\omega\bar{u}_i}{\bar{a}^2}Z_m\frac{\partial Z_l}{\partial x_i} + \frac{\mathrm{i}\omega}{\bar{a}^2}\left(\mathrm{i}\omega Z_m + \bar{u}_i\frac{\partial Z_m}{\partial x_i}\right)Z_l\right\}\phi_m''\bar{\rho}h\,\mathrm{d}A \\
&+ \int\left\{-\mathrm{i}\omega h\left(\delta_{ij} - \frac{\bar{u}_i\bar{u}_j}{\bar{a}^2}\right)\frac{\partial Z_l}{\partial x_i}\zeta_j + \frac{\omega^2 h}{\bar{a}^2}\zeta_j\bar{u}_j Z_l + \bar{u}_i\zeta_j\frac{\partial Z_l}{\partial x_i}\frac{\partial h}{\partial x_j} - \mathrm{i}\omega\frac{\partial h}{\partial x_k}\zeta_k Z_l\right\}\bar{\rho}\,\mathrm{d}A \\
&= \int q_i'' n_i Z_l\,\mathrm{d}s.
\end{aligned} \tag{25}$$

The terms proportional to ϕ''_m give

$$K_{lm}\phi''_m, \tag{26}$$

where

$$K_{lm}=\left\{\left(\delta_{ij}-\frac{\bar{u}_i\bar{u}_j}{\bar{a}^2}\right)\frac{\partial Z_l}{\partial x_i}\frac{\partial Z_m}{\partial x_j}+\frac{i\omega\bar{u}_i}{3\bar{a}^2}\left(\frac{\partial Z_m}{\partial x_i}-\frac{\partial Z_l}{\partial x_i}\right)-\frac{\omega^2}{12\bar{a}^2}(1+\delta_{lm})\right\}\bar{\rho}hA, \tag{27}$$

since when the integral over the triangular element is performed, $\partial Z_l/\partial x_i$ is constant and

$$\int Z_l \mathrm{d}A=\tfrac{1}{3}A, \tag{28}$$

$$\int Z_l Z_m \mathrm{d}A=\tfrac{1}{12}A(1+\delta_{lm}). \tag{29}$$

There is an analogy with structural problems, in which load corresponds to unsteady flow and structural deflection corresponds to unsteady potential, so that K_{lm} will be referred to as a stiffness matrix.

Whilst this is satisfactory in subsonic flow, for supersonic flow it requires to be stabilized, just as for the steady calculation, by using upwind densities. Here only the most elementary upwinding scheme will be used, in which the density is taken in whole from the next element upstream instead of from the element under consideration. This corresponds to an artificial viscosity factor (v) of unity and was used for simplicity of programming. Results for steady flow[3] suggest that much sharper shock and wave effects could be obtained by using an artificial viscosity factor which varied with mean flow Mach number, in the same way as was used for steady flow. A superscript asterisk indicates an upwinded quantity. Only the quasi-steady terms independent of ω are upwinded. The expression (26) is therefore replaced by

$$K_{lm}\phi''_m+K^*_{lm}\phi''^*_m, \tag{30}$$

where

$$K_{lm}=\left\{\frac{\partial Z_l}{\partial x_i}\frac{\partial Z_m}{\partial x_i}+\frac{i\omega\bar{u}_i}{3\bar{a}^2}\left(\frac{\partial Z_m}{\partial x_i}-\frac{\partial Z_l}{\partial x_i}\right)-\frac{\omega^2}{12\bar{a}^2}(1+\delta_{lm})\right\}\bar{\rho}^*hA \tag{31}$$

and

$$K^*_{lm}=-\frac{\bar{u}_i\bar{u}^*_j}{\bar{a}^{*2}}\frac{\partial Z_l}{\partial x_i}\left(\frac{\partial Z_m}{\partial x_j}\right)^*\bar{\rho}^*hA. \tag{32}$$

Turning to the second integral in equation (25), containing terms proportional to ζ, the terms involving $\partial h/\partial x$ are assumed to be small and will be neglected. The following integrals are used:

$$\int\zeta_k \mathrm{d}A=A\begin{bmatrix}1 & 0 & -\bar{y}\\ 0 & 1 & +\bar{x}\end{bmatrix}R_n, \tag{33}$$

$$\int\zeta_k Z_l \mathrm{d}A=A\begin{bmatrix}1/3 & 0 & -(y_l+3\bar{y})/12\\ 0 & 1/3 & +(x_l+3\bar{x})/12\end{bmatrix}R_n, \tag{34}$$

where $\bar{x}$ and $\bar{y}$ are the co-ordinates of the centroid of the element, and

$$R_n=\begin{bmatrix}\xi_x\\ \xi_y\\ \alpha\end{bmatrix}. \tag{35}$$

The complete result of integrating equation (25) over the triangular element is then

$$K_{lm}\phi''_m + K^*_{lm}\phi''^*_m + F_{ln}R_n = \int n_i q''_i Z_l \mathrm{d}s, \tag{36}$$

where

$$\begin{aligned} F_{ln} = &-\mathrm{i}\omega\bar{\rho}hA\left[\frac{\partial Z_l}{\partial x}, \frac{\partial Z_l}{\partial y}, \left(-\bar{y}\frac{\partial Z_l}{\partial x} + \bar{x}\frac{\partial Z_l}{\partial y}\right)\right] \\ &+\mathrm{i}\omega\bar{\rho}hA\left(\frac{\bar{u}_i}{\bar{a}^2}\frac{\partial Z_l}{\partial x_i}\right)\left[\bar{u}_x, u_y, (-\bar{y}\bar{u}_x + \bar{x}\bar{u}_y)\right] \\ &+\frac{1}{12}\frac{\omega^2\bar{\rho}hA}{\bar{a}^2}\left[4\bar{u}_x, 4\bar{u}_y, \{-(y_l+3\bar{y})\bar{u}_x + (x_l+3\bar{x})\bar{u}_y\}\right]. \end{aligned} \tag{37}$$

The $F_{ln}R_n$ term behaves as a source term distributed over the whole field, owing to the incorporation in ϕ'' of terms depending on the blade motion. It is zero in quasi-steady flow, $\omega \to 0$.

In the assembly process the equations for a node L for all triangular elements meeting at L are added together. Then the surface integral on the right-hand side of equation (36) cancels for all internal nodes, but has to be considered at the surfaces of the box and in the wake. By equation (17) it is zero at the blade surface.

FLOW CORRECTION INTEGRAL

The boundary conditions on the surface of the box will be applied in terms of q'_i rather than q''_i. So in evaluating the right-hand side of equation (36), the following integral is required:

$$\begin{aligned} \int n_i(q''_i - q'_i)Z_l \mathrm{d}s &= \int n_i\left(\zeta_k\frac{\partial \bar{q}_i}{\partial x_k} + \bar{q}_k\frac{\partial \zeta_k}{\partial x_i} - \bar{\rho}h\frac{\partial \zeta_i}{\partial t}\right)Z_l \mathrm{d}s \\ &= \int Z_l \mathrm{d}(\zeta_x\bar{q}_y - \zeta_y\bar{q}_x) - \mathrm{i}\omega\int \bar{\rho}n_i\zeta_i Z_l h \mathrm{d}s. \end{aligned} \tag{38}$$

In evaluating the equations for a node L on the boundary of the box (see Figure 2), these integrals have to be evaluated from A to D. Z_l varies linearly from zero at A to unity at L to zero at D. The following integrals are required:

$$\int_{\mathrm{ALD}} Z_l \mathrm{d}\bar{q}_i = -(\bar{q}_i)_{\mathrm{AL}} + (\bar{q}_i)_{\mathrm{LD}}, \tag{39}$$

$$\int_{\mathrm{ALD}} Z_l \mathrm{d}(x_i\bar{q}_i) = -(\bar{q}_i)_{\mathrm{AL}}\tfrac{1}{2}(x_{i\mathrm{A}} + x_{i\mathrm{L}}) + (\bar{q}_i)_{\mathrm{LD}}\tfrac{1}{2}(x_{i\mathrm{L}} + x_{i\mathrm{D}}), \tag{40}$$

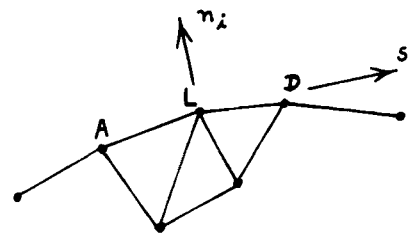

Figure 2. Evaluation of boundary integral

$$\int_{ALD} Z_l \bar{\rho} h \, dx_i = \tfrac{1}{2}(\bar{\rho}h)_{AL}(x_{iL} - x_{iA}) + \tfrac{1}{2}(\bar{\rho}h)_{LD}(x_{iD} - x_{iL}), \tag{41}$$

$$\int_{ALD} Z_l \bar{\rho} h x_i \, dx_i = \tfrac{1}{6}(\bar{\rho}h)_{AL}(x_{iL} - x_{iA})(x_{iA} + 2x_{iL}) + \tfrac{1}{6}(\bar{\rho}h)_{LD}(x_{iD} - x_{iL})(x_{iD} + 2x_{iL}). \tag{42}$$

The result may be written

$$\int n_i(q_i'' - q_i')Z_l \, ds = FC_{ln}R_n, \tag{43}$$

where

$$\begin{aligned} FC_{ln} = &-[\bar{q}_y, -\bar{q}_x, -\tfrac{1}{2}(x_A + x_L)\bar{q}_x - \tfrac{1}{2}(y_A + y_L)\bar{q}_y]_{AL} \\ &+[\bar{q}_y, -\bar{q}_x, -\tfrac{1}{2}(x_L + x_D)\bar{q}_x - \tfrac{1}{2}(y_L + y_D)\bar{q}_y]_{LD} \\ &-\tfrac{1}{2}i\omega(\bar{\rho}h)_{AL}[-(y_L - y_A), (x_L - x_A), \tfrac{1}{3}\{(x_L - x_A)(x_A + 2x_L) + (y_L - y_A)(y_A + 2y_L)\}] \\ &-\tfrac{1}{2}i\omega(\bar{\rho}h)_{LD}[-(y_D - y_L), (x_D - x_L), \tfrac{1}{3}\{(x_D - x_L)(2x_L + x_D) + (y_D - y_L)(2y_L + y_D)\}]. \end{aligned} \tag{44}$$

CONDITIONS AT THE REPEAT BOUNDARY

Figure 3 shows nodes A, L and D on the bottom (suffix b) boundary of the domain, and corresponding nodes A_t, L_t and D_t on the top (suffix t) boundary. Since there is a blade-to-blade phase angle β, every unsteady quantity on the top boundary corresponds to the same quantity on the bottom boundary, multiplied by $\exp(i\beta)$. Hence

$$\phi_t' = \phi_b' \exp(i\beta) \tag{45}$$

and

$$(q_i')_t = (q_i')_b \exp(i\beta). \tag{46}$$

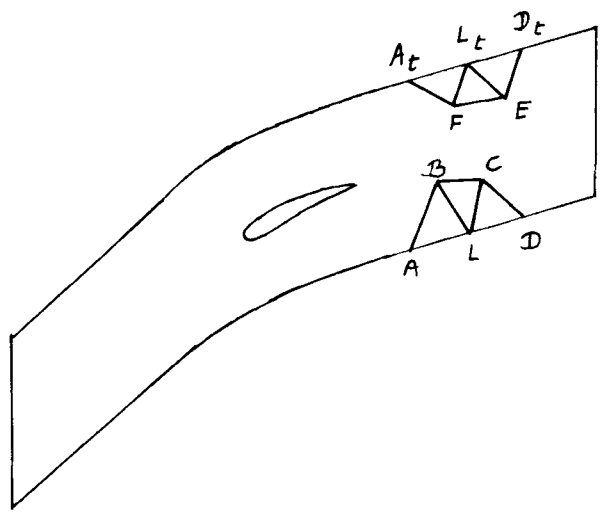

Figure 3. Repeat boundary condition

The corresponding condition on ϕ'' is, from equation (12),

$$\phi''_t - (\zeta_i)_t \bar{u}_i = \{\phi''_b - (\zeta_i)_b \bar{u}_i\} \exp(i\beta). \tag{47}$$

Since $x_t = x_b$, $y_t = y_b + s$ and $(\bar{u}_i)_t = (\bar{y}_i)_b$, this reduces to

$$\phi''_t = (\phi''_m - CP_{mn} R_n) \exp(i\beta), \tag{48}$$

where

$$CP_{mn} = [\bar{u}_x\{1 - \exp(-i\beta)\}, \bar{u}_y\{1 - \exp(-i\beta)\}, (x_t \bar{u}_y - y_t \bar{u}_x)\{1 - \exp(-i\beta)\} + \bar{u}_x s]. \tag{49}$$

The procedure for assembling the equations is to add together all the equations (36) relating to node L for all the elements meeting at L, and then to add together all the equations (36) relating to node L_t. The system relating to node L_t is then multiplied by $\exp(-i\beta)$ and added to the system relating to node L. The result is

$$\left\{\sum_t K_{lm}\phi''_m + \sum_t K^*_{lm}\phi''^*_m + \sum_t F_{ln}R_n\right\}\exp(-i\beta) + \left\{\sum_b K_{lm}\phi''_m + \sum_b K^*_{lm}\phi''^*_m + \sum_b F_{ln}R_n\right\}$$

$$= \int_{ALD} n_i q''_i Z_l \, ds + \int_{A_t L_t D_t} n_i q''_i \exp(-i\beta) Z_l \, ds \tag{50}$$

$$= \{(FC_{ln})_b + (FC_{ln})_t \exp(-i\beta)\} R_n, \tag{51}$$

using equations (43) and (46).

The values of ϕ''_t on the top surface of the domain are eliminated using equation (48), and the terms introduced by the second term on the right-hand side of this equation will be referred to as 'potential correction terms'. The result can be written in the form

$$\sum K_{lm}\phi''_m + \sum K^*_{lm}\phi''^*_m = \left(-\sum F_{ln} + FC_{ln} + PC_{ln}\right) R_n. \tag{52}$$

The stiffness matrices K and K^* are assembled for elements on the top of the domain as if the suffices referred to the corresponding nodes on the bottom of the domain, and according to the following rules.

If l and m both refer to nodes on the top of the domain, then K_{lm} is used.

If l is on the top of the domain and m is internal, then $\exp(-i\beta)K_{lm}$ is used.

If l is internal and m is on the top of the domain, then $\exp(i\beta)K_{lm}$ is used.

For the source terms and flow correction terms, if l refers to a node on the top of the domain, $\exp(-i\beta)F_{ln}$ and $\exp(-i\beta)FC_{ln}$ are used.

For the potential correction terms, if l and m both refer to nodes on the top of the domain,

$$PC_{ln} = K_{lm} CP_{mn}, \tag{53}$$

and if l refers to an internal node and m is on the top,

$$PC_{ln} = K_{lm} CP_{mn} \exp(i\beta). \tag{54}$$

BOUNDARY CONDITIONS ACROSS THE WAKE

The conditions to be applied across the wake are that the flow must be continuous across the wake,

$$\Delta(n_i q'_i) = \Delta(n_i q''_i) = 0, \tag{55}$$

and that the pressure must be continuous across the wake, so that

$$\Delta p' = \left(\frac{\partial}{\partial t} + \bar{u}_j \frac{\partial}{\partial x_j}\right)(\Delta\phi') = 0, \tag{56}$$

where Δ refers to the difference between the bottom and top of the wake.

It will be assumed that the wake lies along a straight line from the trailing edge (suffix te) and that the steady velocity is constant and equal to the steady velocity far downstream (denoted by suffix 2). This leads to

$$\Delta\phi' = \Delta\phi'' = (\Delta\phi'')_{te} \exp\{-i\omega(x - x_{te})/\bar{u}_{x2}\}. \tag{57}$$

In the assembly process, the equations for a node on the top of the wake are added to the equations for a node on the bottom of the wake, and by equation (55) the flow integrals cancel. Equation (57) may then be used to eliminate ϕ'' on the bottom of the wake. The result is that reference to a node m on the top of the wake is treated as if the node were on the bottom of the wake, and

$$K_{lm} \exp\{-i\omega(x_m - x_{te})/\bar{u}_{x2}\} \text{ is added to } K_{l1}$$

and

$$-K_{lm} \exp\{-i\omega(x_m - x_{te})/\bar{u}_{x2}\} \text{ is added to } K_{l(NP-1)}.$$

Here suffix 1 refers to a node on the bottom surface of the blade at the trailing edge, and suffix $(NP-1)$ refers to a node on the top surface at the trailing edge.

In subsonic flow this procedure automatically satisfies the Kutta condition at the trailing edge, since it makes the pressures in the two elements adjoining the cusp behind the trailing edge very nearly equal. In supersonic flow, however, there is usually a sudden change in pressure between the elements which include a node at the trailing edge.

BOUNDARY CONDITIONS AT INLET

The boundary conditions at the inlet face are found by matching the solution to a linearized analytic solution obtained by assuming that the mean flow conditions are uniform. This analytic solution is given by

$$\phi' = \sum_{r=r_1}^{r_N} C_r \exp\{i(\hat{\alpha}x + \hat{\beta}y)\}, \tag{58}$$

where C_r are constants.

The wave number in the tangential direction, $\hat{\beta}$, must be chosen to satisfy the required blade-to-blade phase angle β, so that

$$\hat{\beta} = (\beta + 2\pi r)/s, \tag{59}$$

where r is an integer.

Substitution in the convected wave equation shows that the wave number in the axial direction, $\hat{\alpha}$, is given by

$$\hat{\alpha} = \{(\omega/\bar{a} + \hat{\beta}M_y)M_x \pm (-D)^{1/2}\}/(1 - M_x^2), \tag{60}$$

where

$$D = (1 - M_x^2)\hat{\beta}^2 - (\omega/\bar{a} + \hat{\beta}M_y)^2, \tag{61}$$

and the Mach number components are given by

$$M_x = \bar{u}_x/\bar{a}, \tag{62}$$

$$M_y = \bar{u}_y/\bar{a}. \tag{63}$$

If D is positive, then equation (60) shows two complex values of $\hat{\alpha}$. The negative sign gives a solution which grows exponentially in the direction of x increasing, and this is the root required on the upstream face.

If D is negative, then there are two real roots for $\hat{\alpha}$ corresponding to two propagating waves. One root corresponds to a wave carrying energy axially upstream, and this is the root required on the upstream face. The other root corresponds to a wave carrying energy downstream, and this is the root required on the downstream face. On the upstream face, if $(\omega/\bar{a}+\hat{\beta}M_y)$ is positive, the positive sign in equation (60) is required, and if $(\omega/\bar{a}+\hat{\beta}M_y)$ is negative, the negative sign is required.

When D is zero, the resonance or cut-off condition occurs, and near this point the results from the program are found to exhibit wild fluctuations.

The unsteady axial flow perturbation is given by

$$q'_x = \sum_{r=r_1}^{r_N} \pm(-D)^{1/2} \mathrm{i}\bar{\rho}hC_r \exp\{\mathrm{i}(\hat{\alpha}x+\hat{\beta}y)\}, \tag{64}$$

where the choice of sign is made in the same way as for equation (60).

If there are N elements adjoining the upstream boundary (so that counting both corner points there are $N+1$ nodes), then N terms of the series in equations (58) and (64) can be used to match the finite element solution. r_1 and r_N are chosen so that those terms with the largest possible wavelength in the y-direction, and therefore least $|\hat{\beta}|$, are used.

Equation (58) gives the unsteady potentials at the nodes on the inlet face. Node l, $1 \leqslant l \leqslant N$, is at $(x_{\mathrm{BL}}, y_{\mathrm{BL}}+(l-1)s/N)$, where the suffix BL indicates the node at the bottom left corner of the mesh. So

$$[\phi'_l] = [\exp(\mathrm{i}\beta_l/N)][\exp(\mathrm{i}2\pi rl/N)][C_r \exp\{\mathrm{i}(\hat{\alpha}x_{\mathrm{BL}}+\hat{\beta}y_{\mathrm{BL}}-\hat{\beta}s/N)\}]. \tag{65}$$

Inversion of the matrix in the second factor gives

$$[\exp(\mathrm{i}2\pi rl/N)]^{-1} = (1/N)[\exp(-\mathrm{i}2\pi lr/N)],$$

so that

$$[C_r \exp\{\mathrm{i}(\hat{\alpha}x_{\mathrm{BL}}+\hat{\beta}y_{\mathrm{BL}}-\hat{\beta}s/N)\}] = (1/N)[\exp(-\mathrm{i}\hat{\beta}sm/N)][\phi'_m]. \tag{66}$$

The flow integral for node l (see Figure 2) is, using equation (64), given by

$$\int_A^D n_i q'_i Z_l \mathrm{d}s = \sum_{r=r_1}^{r_N} \pm(-D)^{1/2} \mathrm{i}\bar{\rho}hC_r \exp[\mathrm{i}\{\hat{\alpha}x_{\mathrm{BL}}+\hat{\beta}y_{\mathrm{BL}}+\hat{\beta}(l-1)s/N\}](s/N)F(\hat{\beta}s/N), \tag{67}$$

where

$$F(\theta) = (1-\cos\theta)/(\tfrac{1}{2}\theta^2). \tag{68}$$

The function $F(\theta)$ has the effect of attenuating the terms with the higher values of $|\hat{\beta}|$. It is similar to, but less drastic than, the σ-function used by Lanczos[9] to mitigate the effects of truncating a Fourier series.

C_r may be eliminated from equations (66) and (67) to give

$$\int_A^D n_i q'_i Z_l \mathrm{d}s = K^{\mathrm{u}}_{lm} \phi'_m \tag{69}$$

where K^{u}_{lm} is the stiffness matrix for the upstream region, regarded as a finite element with N nodes, given by

$$K^{u}_{lm}=\sum_{r=r_1}^{rN} \pm(-D)^{1/2}\mathrm{i}\bar{\rho}h(s/N^2)\exp\{\mathrm{i}(l-m)\hat{\beta}s/N\}F(\hat{\beta}s/N). \tag{70}$$

When the equations are assembled for a node on the inlet face, the result is

$$\sum K_{lm}\phi''_m+\sum K^{*}_{lm}\phi''^{*}_m+K^{u}_{lm}\phi''_m=\left(-\sum F_{ln}+FC_{ln}+PC_{ln}\right)R_n, \tag{71}$$

where the flow correction (FC) is given by equation (44), and the potential correction is

$$PC_{ln}=[\bar{u}_{x1},\bar{u}_{y1},(x_l\bar{u}_{y1}-y_l\bar{x}_{x1})]. \tag{72}$$

BOUNDARY CONDITIONS AT OUTLET

Behind the exit face there is a potential field exactly similar to that ahead of the inlet face. There is one change of sign to select the waves decaying or propagating downstream, and another because the vector n_i points in the opposite direction. Equation (70) therefore also applies for the downstream region.

In addition there is a field due to the vortex sheets shed from the trailing edge of each blade. The potential jump across the wake vortex sheets ($\Delta\phi'$) is given by equation (57). To analyse this field it is convenient to take axes Ox' and Oy', parallel and perpendicular to the mean flow, at an angle α_2 to the axial direction, and with a velocity $\bar{u}_2$. The origin for these axes is taken at the point where the wake from the reference blade crosses the outlet plane, as shown on Figure 4. All unsteady

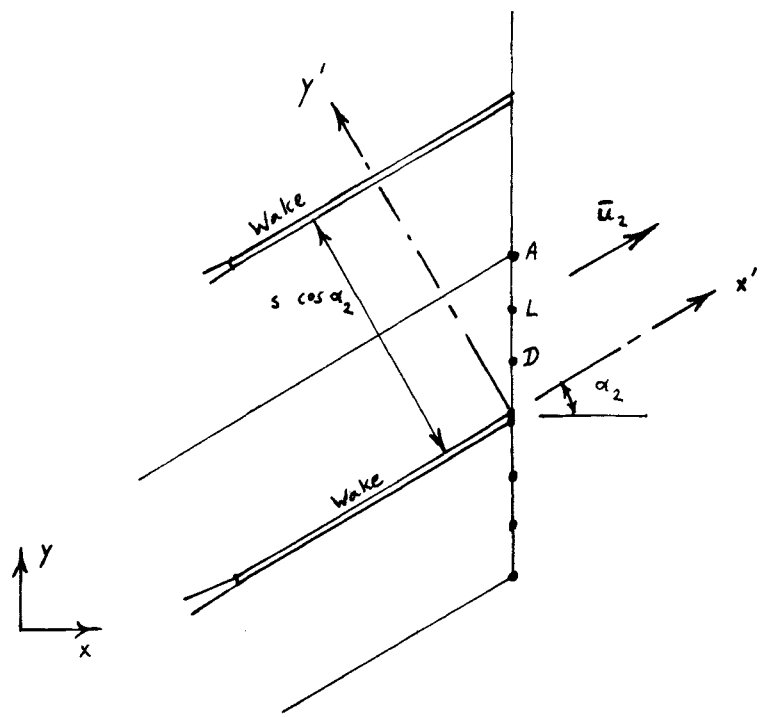

Figure 4. Outlet boundary

variables are convected at the mean flow velocity and are proportional to $\exp\{i\omega(t-x'/\bar{u}_2)\}$. This flow has no pressure or density fluctuations, so that it is effectively incompressible and satisfies $\nabla^2\phi'=0$. The required solution in the region $0<y'<s\cos\alpha_2$, satisfying continuity of velocity normal to the wake and giving the correct $\Delta\phi'$, is

$$\phi'=\{C_1\exp(\omega y'/\bar{u}_2)+C_2\exp(-\omega y'/\bar{u}_2)\}\exp(-i\omega x'/\bar{u}_2)(\Delta\phi')_2, \tag{73}$$

where

$$C_1=\{\exp(iP)-\exp(-Q)\}/4(\cosh Q-\cos P), \tag{74}$$

$$C_2=\{\exp(iP)-\exp(+Q)\}/4(\cosh Q-\cos P), \tag{75}$$

$$P=(\omega s/\bar{u}_2)\sin(\alpha_2)+\beta, \tag{76}$$

$$Q=(\omega s/\bar{u}_2)\cos(\alpha_2) \tag{77}$$

and $(\Delta\phi')_2$ is the potential jump at the exit face.

The potential at a node l on the exit face, where $x'=ls\sin\alpha_2/N$ and $y'=ls\cos\alpha_2/N$, is then given by

$$\phi'_l=f_l(\Delta\phi')_2, \tag{78}$$

where

$$f_l=C_1\exp(l\xi)+C_2\exp(-l\xi^*), \quad 0\leqslant l\leqslant N, \tag{79}$$

$$\xi=(\omega s/\bar{u}_2N)(\cos\alpha_2-i\sin\alpha_2), \tag{80}$$

$$\xi^*=(\omega s/\bar{u}_2N)(\cos\alpha_2+i\sin\alpha_2).$$

For negative l,

$$f_l=f_{l+n}\exp(-i\beta), \quad -N\leqslant l\leqslant 0. \tag{81}$$

For $l=0$ these equations give two values of f_0, differing by unity, one of which applies just above the wake and the other just below.

The corresponding flow across the exit face is given by

$$q'_x=\bar{\rho}h\frac{\partial\phi'}{\partial x}. \tag{82}$$

This gives the flow integral for a node l (see Figure 4) as

$$\int_A^D n_i q'_i Z_l \mathrm{d}s=g_l(\Delta\phi')_2, \tag{83}$$

where

$$\begin{aligned}
g_l&=i\bar{\rho}h[C_1\exp(l\xi)\{\exp(\xi)+\exp(-\xi)-2\}/\xi\\
&\quad+C_2\exp(-l\xi^*)\{\exp(\xi^*)+\exp(-\xi^*)-2\}/\xi^*], \quad 1\leqslant l<N,\\
g_l&=g_{l+n}\exp(-i\beta), \quad -N<l\leqslant -1,\\
g_0&=i\bar{\rho}h[C_1\{\exp(\xi)-1-\xi\}/\xi+C_2\{\exp(-\xi^*)-1+\xi^*\}/\xi^*]\\
&\quad+\text{complex conjugate term.}
\end{aligned} \tag{84}$$

The potential from the combined acoustic wave and vortex sheet solutions is then

$$\phi'_l = \sum C_r \exp\{i(\hat{\alpha} x_l + \hat{\beta} y_l)\} + (\Delta\phi')_2 f_l. \tag{85}$$

Eliminating the constant C_r, as for the inlet duct, gives for the flow integral

$$\int_A^D n_i q'_i Z_l \mathrm{d}s = K^u_{lm}\{\phi'_m - (\Delta\phi')_2 f_m\} + g_l(\Delta\phi')_2$$
$$= K^u_{lm}\phi'_m + (g_l - K^u_{lm} f_m)\exp\{-i\omega(x_m - x_{te})/\bar{u}_{x2}\}(\Delta\phi')_{te}. \tag{86}$$

When the equations are assembled for a node on the exit face, the result is

$$\sum K_{lm}\phi''_m + \sum K^*_{lm}\phi''^*_m + K^u_{lm}\phi''_m + (g_l - K^u_{lm} f_m)\exp\{-i\omega(x_m - x_{te})/\bar{u}_{x2}\}(\phi''_1 - \phi''_{NP-1})$$
$$= \left(-\sum F_{ln} + FC_{ln} + PC_{ln}\right) R_n, \tag{87}$$

where the flow correction (FC) and the potential correction (PC) are obtained from equations (44) and (72) as before.

BLADE FORCES AND MOMENT

The result of assembling equations (36) for each element, together with the equations for the boundary conditions such as (52), (71) and (87), is a set of linear equations for the unknown ϕ'' at each node. These equations are solved by Gaussian elimination. The nodes are renumbered in such a way that the large stiffness matrix K is banded, with a consequent large reduction in the amount of computer storage required for this matrix.

Once ϕ'' has been found, the pressure on the surface is obtained from equation (15). The unsteady forces (in the axial and tangential directions) and moment (positive anticlockwise about the origin of co-ordinates) per unit blade height are then given by

$$F'_x = \oint p'_s \, \mathrm{d}y - \bar{F}_y \alpha, \tag{88}$$

$$F'_y = -\oint p'_s \mathrm{d}x + \bar{F}_x \alpha, \tag{89}$$

$$M' = -\oint p'_s (x\,\mathrm{d}x + y\,\mathrm{d}y), \tag{90}$$

where the integrals are taken clockwise round the blade surface. The second terms in equations (88) and (89) are due to the rotation of the steady blade forces by an amount equal to the rotation of the blade.

The final result from the program is a set of nine complex non-dimensional coefficients (C) which give the forces and moment as follows

$$C = \begin{bmatrix} C_{xx} & C_{xy} & C_{x\alpha} \\ C_{yx} & C_{yy} & C_{y\alpha} \\ C_{Mx} & C_{My} & C_{M\alpha} \end{bmatrix} = \begin{bmatrix} F'_x/\bar{\rho}_1\bar{u}_1^2\xi_x & F'_x/\bar{\rho}_1\bar{u}_1^2\xi_y & F'_x/\bar{\rho}_1\bar{u}_1^2 c\alpha \\ F'_y/\bar{\rho}_1\bar{u}_1^2\xi_x & F'_y/\bar{\rho}_1\bar{u}_1^2\xi_y & F'_y/\bar{\rho}_1\bar{u}_1^2 c\alpha \\ M'/\bar{\rho}_1\bar{u}_1^2 c\xi_x & M'/\bar{\rho}_1\bar{u}_1^2 c\xi_y & M'/\bar{\rho}_1\bar{u}_1^2 c^2\alpha \end{bmatrix}. \tag{91}$$

In some of the results to be quoted for cascades of flat plates or zero-camber cascades, force coefficients C_{Lh} and $C_{L\alpha}$, which refer to the force normal to the blade chord, and a moment coefficient C_{Mh} are used, where suffix h here refers to translational motion normal to the chord.

RESULTS

Comparison between some results from various versions of this program and other theoretical results will be given next. These are all for strictly two-dimensional flow ($h = 1$). Other comparisons with theoretical and experimental work have been made by Bölcs and Fransson,[10] and a comparison with some moderate-quality experimental transonic data has been given by Davies and Whitehead.[11] These comparisons will not be repeated here.

Figures 5 and 6 show the real and imaginary parts of the jump in unsteady pressure across the blades in a flat plate cascade. The FINSUP program results are compared with results from a linearized flat plate program, LINSUB, based on theory by Smith.[12] The program has been given by Whitehead.[1] This is for incompressible flow at the rather high frequency parameter of 6. The agreement between the two programs is excellent.

Figures 7 and 8 show unsteady pressures for a cascade of biconvex zero-camber blades. The FINSUP program results are compared with results from a singularity theory by Atassi and Akai.[13] This is for incompressible flow at 2·1° incidence, and for bending vibration with amplitude a normal to the chord. Again the agreement is excellent.

Figure 9 shows a comparison with results by Verdon.[14] This is for a cascade of NACA 0006 aerofoils, and the flow is subsonic throughout. This again is for bending vibration with amplitude a normal to the chord. The figure shows a work coefficient defined by

$$W_c = \frac{\text{work done per cycle per unit blade length}}{\bar{\rho}_1 \bar{u}_1^2 a^2} \tag{92}$$

plotted against inter-blade phase angle. If this work coefficient goes positive, then flutter is

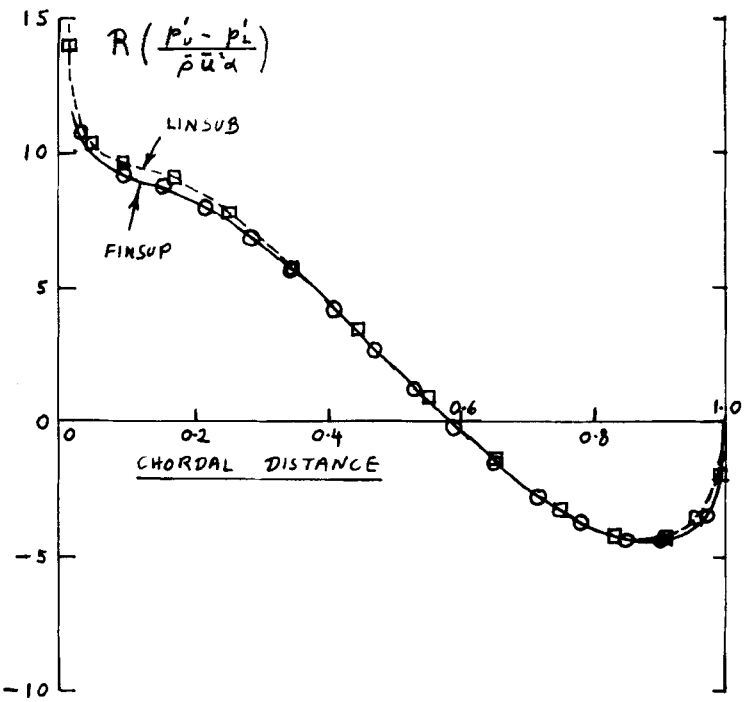

Figure 5. Flat plate cascade. Torsion about mid-chord. $s/c = 0{\cdot}75$, stagger $= 60°$, $M = 0$, $\omega c/u_1 = 6$, $\beta = 270°$

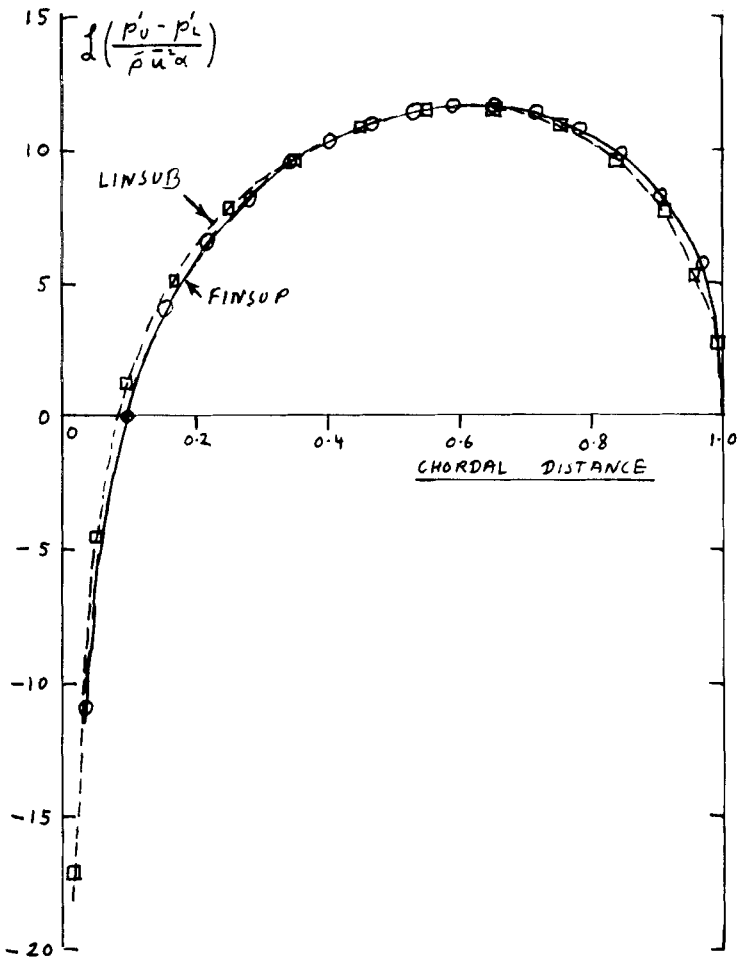

Figure 6. Flat plate cascade. Torsion about mid-chord. $s/c = 0{\cdot}75$, stagger $= 60°$, $M = 0$, $\omega c/\bar{u}_1 = 6$, $\beta = 270°$

predicted for a cascade of perfectly tuned blades having no mechanical damping. The prominent kinks in these curves are due to acoustic resonances in the inlet and outlet ducts. The results show generally satisfactory agreement, although Verdon's acoustic resonance effects appear to be slightly more drastic than those from FINSUP, and there are some appreciable differences near resonances at the higher frequencies.

Turning to results with supersonic flow, Figure 10 shows a comparison with quasi-steady analytic results for supersonic uniform steady flow in a cascade of flat plates which has been previously used by Verdon and McCune.[15] The theory has been given, for instance, by Whitehead.[1] This is for torsional vibration about an axis at mid-chord. A wave propagating upwards from the leading edge is reflected from the lower surface of the next blade above at 68% chord, and gives a discontinuity in pressure at this point. The FINSUP result shows this pressure rise heavily smeared over a substantial proportion of the blade lower surface. Similarly, a wave propagating downwards from the leading edge passes just behind the trailing edge of the next blade below, missing it by 4% of the chord. The FINSUP result shows the pressure on the upper

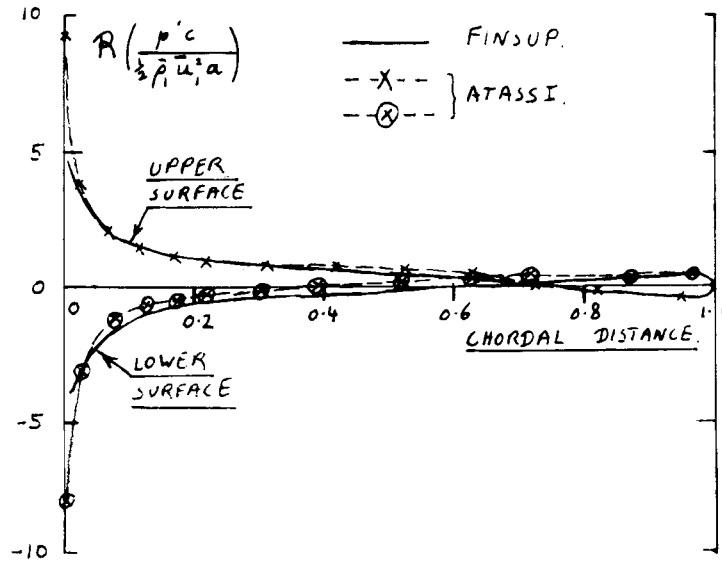

Figure 7. Biconvex profiles. Thickness = 10%, camber = 0, $s/c = 1$, stagger = 45°, $\alpha_1 = 47{\cdot}1°$, $\omega c/\bar{u}_1 = 1$, $\beta = 180°$

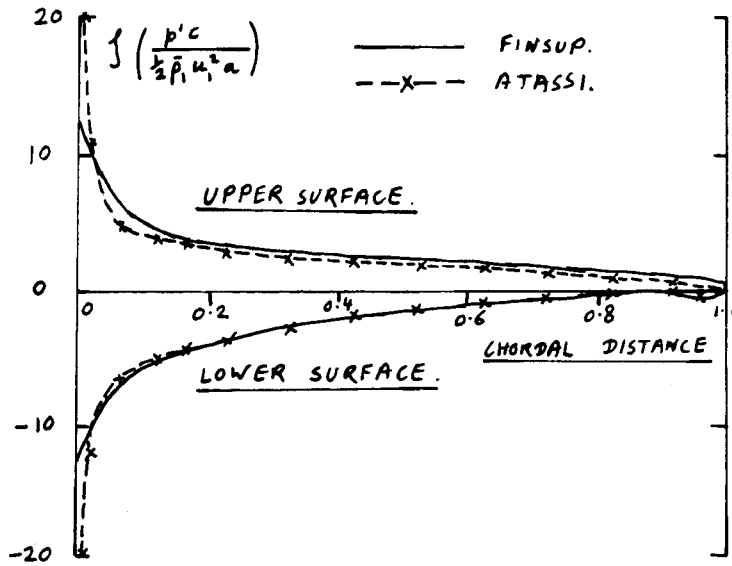

Figure 8. Biconvex profiles. Thickness = 10%, camber = 0, $s/c = 1$, stagger = 45°, $\alpha_1 = 47{\cdot}1°$, $\omega c/\bar{u}_1 = 1$, $\beta = 180°$

surface rising near the trailing edge, in anticipation of the arrival of this wave. Nevertheless, although the details of the unsteady pressure distributions differ quite appreciably, the integrated results for the blade forces and moments agree quite well, as shown in Table I.

Table I also shows similar results for the same cascade at a frequency parameter of 0·6021. In this case they are compared with results from a program LINSUP, based on the theory given by Nagashima and Whitehead.[16] Again the results agree quite well.

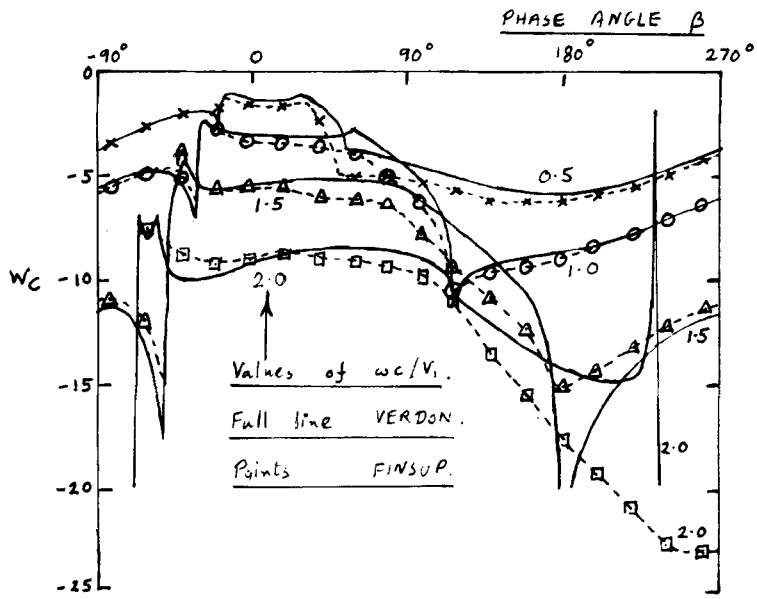

Figure 9. NACA 0006 profile. $s/c = 1$, stagger $= 45°$, $M_1 = 0{\cdot}7$, $\alpha_1 = 55°$

As a final comparison, Figures 11 and 12 show unsteady pressure distributions for the same cascade in the case when a strong normal shock wave stands at entry to the passage and is just upstream of the leading edge of the upper blade. In this case the comparison theory is that due to Goldstein *et al.*,[17] programmed by Acton (unpublished). In this case, when the blades vibrate, the position of the strong normal shock wave also oscillates, and this raises a delta function in the unsteady pressure distribution at the point where the normal shock hits the upper surface of the lower blade. This delta function is not shown in Figures 11 and 12, but it is included in the calculation of lift and moment. The shock is assumed to remain just upstream of the leading edge of the upper blade, so there is no delta function here. On the upper surface the two theories agree well over the front half of the chord, but near the shock position there is disagreement, because FINSUP has included the delta function and spread it over an appreciable proportion of the chord. On the lower surface the Acton program does not see the normal shock at the leading edge, but in FINSUP this has spread onto the blade surface and affected the unsteady pressure distribution near the leading edge. As a result of this, when the unsteady force and moment coefficients are compared, as shown in Table II, the force coefficients show quite appreciable differences, and the agreement for the moment coefficients is rather worse. This is a very severe test, since a small increase in the driving parameter for the steady flow calculation, corresponding to a very small decrease in the static pressure ratio across the cascade, will move the shock into the passage and cause a large change in the unsteady force and moment coefficients.

CONCLUSIONS

The theory presented leads to a computer program which is fast and has moderate storage requirements, so that it can be run on a personal computer. The important features in this respect are the use of a finite element mesh of triangular elements, the use of the modified potential ϕ'' to deal with difficulty in the boundary condition near the leading and trailing edges, and the use of

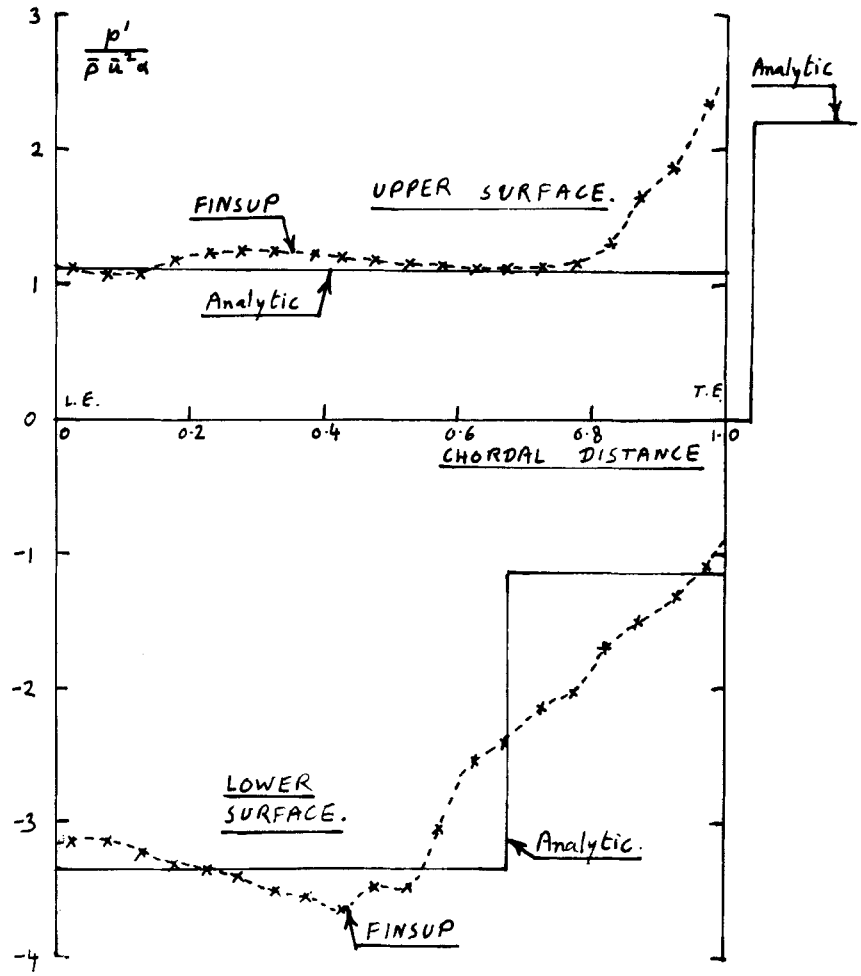

Figure 10. Flat plate cascade. Torsion about mid-chord. $s/c = 0{\cdot}7889$, stagger $= 59{\cdot}53°$, $M_1 = M_2 = 1{\cdot}3453$, $\alpha_1 = \alpha_2 = 59.53°$, $\omega = 0$, $\beta = 180°$

direct matrix division, so that no iteration is necessary. Banded matrix techniques are used to reduce the storage requirement. In the PC implementation it is usually possible to keep the number of matrix elements below 16 000, so that each part of the matrix fits into a single segment of memory, with a substantial saving of calculation time. This is about 5 min for each unsteady case. On a fast mainframe computer, response is essentially immediate. A typical mesh contains about 300 nodes and 500 elements.

Comparisons with other theories in special cases show that the program is very accurate in subsonic flow, and that in supersonic flow, although the wave effects are heavily smeared by the numerical process, the results for overall blade force and moment have acceptable accuracy. This numerical smearing tends to simulate the smearing which occurs on actual blades due to boundary layer effects, but of course the reasons for the smearing are quite different in the two cases, so that the similarity is at most qualitative. Refining the mesh gives improved accuracy, but the reduction of shock smearing is quite small.

Table I. Comparison with analytic and linearized supersonic solutions

Verdon and McCune cascade 'A'
$s/c = 0{\cdot}7889$, stagger $= 59{\cdot}53°$, $M_1 = M_2 = 1{\cdot}3453$, $\alpha_1 = \alpha_2 = 59{\cdot}53°$
Translational vibrational normal to chord
Axis at mid-chord

$\beta = 180{\cdot}0°$, $\omega c/\bar{u}_1 = 0{\cdot}0$	Analytic	FINSUP
$C_{L\alpha}$	$-3{\cdot}73$	$-4{\cdot}04$
$C_{M\alpha}$	$0{\cdot}24$	$0{\cdot}14$
$\beta = 180{\cdot}0°$, $\omega c/\bar{u}_1 = 0{\cdot}6021$	LINSUP	FINSUP
C_{Lh}	$-0{\cdot}83-1{\cdot}69i$	$-0{\cdot}94-1{\cdot}57i$
C_{Mh}	$0{\cdot}17+0{\cdot}04i$	$0{\cdot}02+0{\cdot}13i$
$C_{L\alpha}$	$-2{\cdot}85+1{\cdot}22i$	$-2{\cdot}66+1{\cdot}38i$
$C_{M\alpha}$	$0{\cdot}26-0{\cdot}19i$	$0{\cdot}20-0{\cdot}14i$

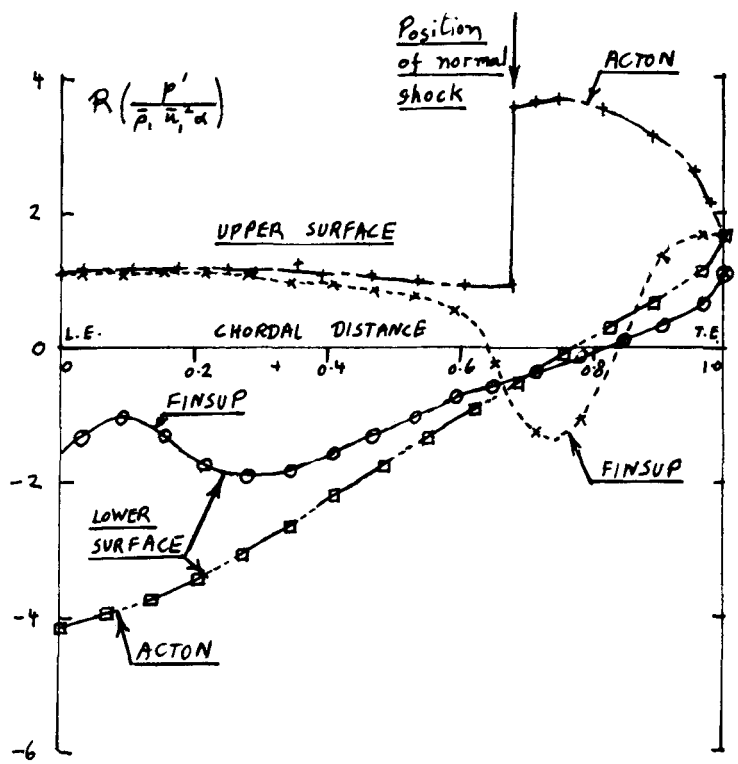

Figure 11. Flat plate cascade. Torsion about mid-chord. $s/c = 0{\cdot}7889$, stagger $= 59{\cdot}53°$, $M_1 = 1{\cdot}34$, $\alpha_1 = 59.53°$, $\omega c/\bar{u}_1 = 0{\cdot}6021$, $\beta = 180°$

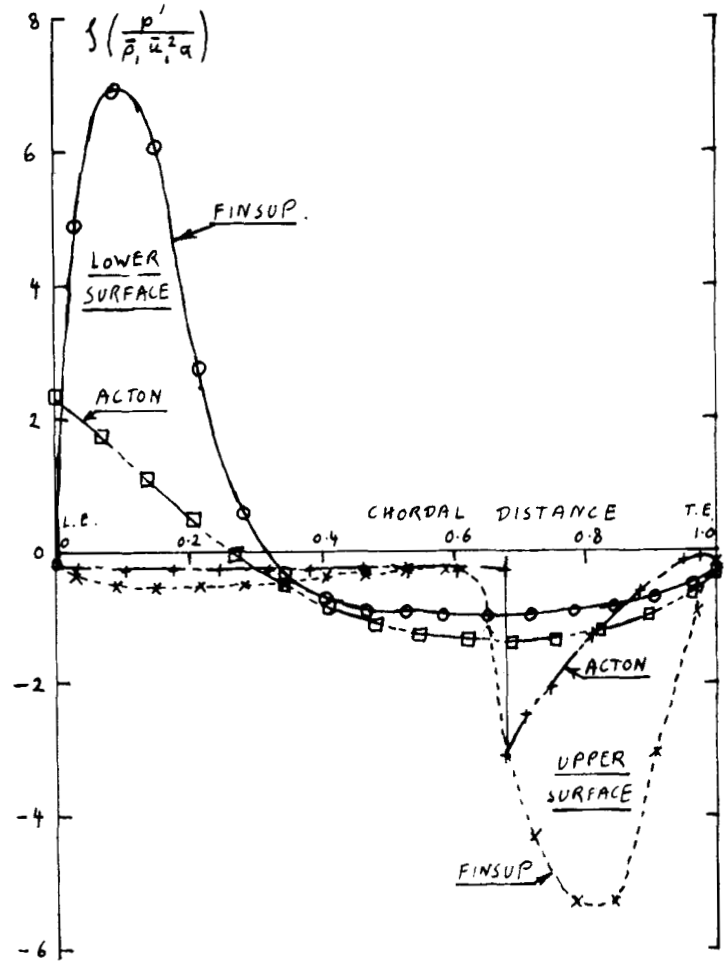

Figure 12. Flat plate cascade. Torsion about mid-chord. $s/c = 0.7889$, stagger $= 59.53°$, $M_1 = 1{\cdot}34$, $\alpha_1 = 59{\cdot}53°$, $\omega c/\bar{u}_1 = 0{\cdot}6021$, $\beta = 180°$

The results from the program can be used for engineering assessment of the stability of actual compressor and turbine blades, for instance as has been done by Whitehead[18] for turbine blades.

ACKNOWLEDGEMENTS

The author makes grateful acknowledgement to Dr. P. Stow, Dr. S. G. Newton and Dr. R. D. Cedar of Rolls-Royce, all of whom made important contributions to this work. The author also makes grateful acknowledgement to Dr. E. Acton (Topexpress), Professor H. Atassi (University of Notre Dame) and Dr. J. M. Verdon (United Technologies Research Center), all of whom made results from their programs available.

Table II. Comparison with Goldstein *et al.*[17]

Verdon and McCune cascade 'A'
$s/c = 0{\cdot}7889$, stagger $= 59{\cdot}53°$
Translational vibrational normal to chord
Axis at mid-chord

$\beta = 180{\cdot}0°$, $\omega c/\bar{u}_1 = 0{\cdot}6021$	Acton program	FINSUP
M_1	1·3454	1·3423
M_2	0·7639	0·7059
α_1	59·53°	59·70°
α_2	59·52°	59·54°
C_{Lh}	$-1{\cdot}65-1{\cdot}44i$	$-2{\cdot}16-0{\cdot}96i$
C_{Mh}	$-0{\cdot}09+0{\cdot}37i$	$0{\cdot}32+0{\cdot}14i$
$C_{L\alpha}$	$-1{\cdot}99+1{\cdot}54i$	$-1{\cdot}49+2{\cdot}29i$
$C_{M\alpha}$	$0{\cdot}51+0{\cdot}08i$	$0{\cdot}27-0{\cdot}27i$

REFERENCES

1. D. S. Whitehead, 'Classical two-dimensional methods', *AGARDograph No. 298. AGARD Manual on Aeroelasticity in Axial-Flow Turbomachines, Vol. 1*, 1987, pp. 3-1–3-30.
2. E. Acton and S. G. Newton, 'Numerical methods for unsteady transonic flow', *AGARDograph No. 298. AGARD Manual on Aeroelasticity in Axial-Flow Turbomachines, Vol. 1*, 1987, pp. 6-1–6-21.
3. D. S. Whitehead and S. G. Newton, 'A finite element method for the solution of two-dimensional transonic flows in cascades', *Int. j. numer. methods fluids*, **5**, 115–132 (1985).
4. D. S. Whitehead, 'The calculation of steady and unsteady transonic flow in cascades', *Cambridge University Engineering Department Report CUED/A-Turbo/TR 118*, 1982.
5. R. D. Cedar and P. Stow, 'The addition of quasi-three-dimensional terms into a finite element method for transonic turbomachinery blade-to-blade flows', *Int. j. numer. methods fluids*, **5**, 101–114 (1985).
6. R. D. Cedar and P. Stow, 'A compatible mixed design and analysis finite element method for the design of turbomachinery blades', *Int. J. numer. methods fluids*, **5**, 331–345 (1985).
7. M. Hart and D. S. Whitehead, 'A design method for two-dimensional cascades of turbomachinery blades', *Int. j. numer. methods fluids*, **7**, 1363–1381 (1987).
8. P. Stow and S. P. Newman, 'Coupled inviscid–boundary layer methods for turbomachinery blading design', *Proc. IMA/SMAI Conf. on Computational Methods in Aeronautical Fluid Dynamics*, University of Reading, April 1987.
9. C. Lanczos, *Applied Analysis*, Pitman, 1957, pp. 219–221.
10. A. Bölcs and T. H. Fransson, 'Aeroelasticity in turbomachines. Comparison of theoretical and experimental cascade results', *EPFL, Lausanne, Report No. 13*, 1986.
11. M. R. D. Davies and D. S. Whitehead, 'Unsteady aerodynamic moment measurement: measurements in a transonic annular cascade', *Proc. Symp. on Unsteady Aerodynamics of Turbomachines and Propellers*, Cambridge, 1984, pp. 487–502.
12. S. N. Smith, 'Discrete frequency sound generation in axial flow turbomachines', *ARC R&M 3709*, 1972.
13. H. Atassi and T. J. Akai, 'Aerodynamic and aeroelastic characteristics of oscillating loaded cascades at low Mach number', *Trans. ASME, J. Eng. Power*, **102**, 344–351 (1980).
14. J. M. Verdon, 'The unsteady aerodynamic response to arbitrary modes of blade motion', *J. Fluids Struct.*, **3**, 255–274 (1989).
15. J. M. Verdon, and J. E. McCune, 'Unsteady supersonic cascade in subsonic axial flow', *AIAA J.* **13**, 193–201 (1975).
16. T. Nagashima and D. S. Whitehead, 'Linearized supersonic unsteady flow in cascades', *ARC R&M 3811*, 1976.
17. M. E. Goldstein, W. Braun and J. J. Adamczyk, 'Unsteady flow in a supersonic cascade with strong in-passage shocks', *J. Fluid Mech.*, **83**, 569–604 (1977).
18. D. S. Whitehead, 'Flutter of turbine blades', *Proc. Symp. on Unsteady Aerodynamics and Aeroelasticity of Turbomachines and Propellers*, RWTH, Aachen, 1987, pp. 437–452.